

Research Article

Tianpeng Li, Jing Fan*, and Tingting Sun

Acid red G dye removal from aqueous solutions by porous ceramsite produced from solid wastes: Batch and fixed-bed studies

<https://doi.org/10.1515/gps-2020-0068>

received August 08, 2020; accepted October 06, 2020

Abstract: A novel porous ceramsite was made of municipal sludge, coal fly ash, and river sediment by sintering process, and the performance of batch and fixed-bed column systems containing this material in the removal of acid red G (ARG) dye from aqueous solutions was assessed in this study. The results of orthogonal test showed that sintering temperature was the most important determinant in the preparation of porous ceramsite, and it possesses developed pore structure and high specific surface area. Batch experiment results indicated that the adsorption process of ARG dye toward porous ceramsite was a spontaneous exothermic reaction, which could be better described with Freundlich–Langmuir isotherm model ($R^2 > 0.992$) and basically followed the pseudo-first-order kinetic equation ($R^2 > 0.993$). Column experiment results showed that when the porous ceramsite was used as packing material, its adsorption capacity was roughly improved by 3.5 times compared with that in batch system, and the breakthrough behavior was simulated well with Yoon–Nelson model, with $R^2 > 0.954$. This study suggested that the novelty man-made porous ceramsite obtained from solid wastes might be processed as

a certain cost-effective treatment material fit for the dye removal in aqueous solutions.

Keywords: porous ceramsite, dye wastewater, adsorption process, breakthrough performance, kinetic analysis

1 Introduction

Ceramsite is a typical porous material, which has many applications in the fields of architecture industry, landscaping area, environmental protection, and so on [1–3], mainly because of its high porosity, large pore diameter, good chemical stability, and sufficient mechanical strength [4,5]. Currently, there are two major preparation processes of ceramsite, such as high-temperature sintering method and sintering-free method [6,7]. Among them, the former has attained widespread application, whereas the latter remains in the stage of technical improvement. It is a routine to use irreplaceable objects represented by clay and shale as a key raw material in the production of ceramsite [8,9]. Undoubtedly, the traditional preparation method is not environmentally friendly, and therefore it cannot meet the requirements of sustainable development [10]. Eventually, it emphasizes the necessity to apply new raw materials in place of irreplaceable objects.

Municipal sludge is an essential by-product generated in drinking water treatment plants and wastewater treatment facilities [11,12]. Generally, municipal sludge contains various organic pollutants (such as polychlorinated biphenyls, polycyclic aromatic hydrocarbons, and dioxins), heavy metals (such as Cr, Hg, and Pb), and pathogenic agents [13,14]. In recent years, the main ways of municipal sludge disposal can be followed by different processes, ranging from agricultural fertilizer, composting, sanitary landfill, and incineration [15,16]. Unfortunately, the aforementioned options have significant drawbacks [17]. For instance, heavy metals in municipal sludge often cause serious environmental problems, restricting its application as a fertilizer. Besides, landfills occupy vast lands and pollute the surroundings. Therefore,

* **Corresponding author: Jing Fan**, School of Environment, Henan Normal University, Xinxiang, Henan 453007, China, e-mail: fanjing@htu.cn, tel: +86-03-73-332-5971, fax: +86-03-73-332-5719

Tianpeng Li: School of Environment, Henan Normal University, Xinxiang, Henan 453007, China; College of City and Architecture Engineering, Zaozhuang University, Zaozhuang, Shandong 277160, China; Shandong Key Laboratory of Water Pollution Control and Resource Reuse, Shandong University, Qingdao, Shandong 266237, China

Tingting Sun: College of Food Science and Pharmaceutical Engineering, Zaozhuang University, Zaozhuang, Shandong 277160, China

it is essential to develop more effective and safer approaches for the municipal sludge disposal. Many studies have proved that the utilization of municipal sludge as a resource is an effective approach to alleviate the pollution [18–20].

Because of similar mineral contents between solid waste and non-renewable natural resource, the combination of solid waste utilization and ceramsite production has been experimentally explored [21–23]. Fabricating ceramsite from solid wastes can not only improve solid wastes management, but also conserve valuable natural resources. The novel ceramsite can be used as water treatment materials, such as absorbents, recyclable bulking agents, catalyst support materials, or packing materials [24,25]. However, the comparative study on ceramsite produced from solid wastes between the batch and fixed-bed column in the performance of organic pollutants removal from aqueous solutions has not been reported.

Wastewater from textile industry has been widely acknowledged as a prime pollution source across the globe [26,27]. It will cause serious environmental problems, such as pollution of water resource, threat to the ecology environment, and even toxic to human beings [28,29]. Anionic dye is one of the major dyes normally used in textile industry, which is composed of anionic ions and sometimes referred to as anionic dye. Acid red G (ARG) dye is an example of anionic dye, with molecular formula $C_{18}H_{15}N_3Na_2O_8S_2$ and molecular weight 509.42 g/mol. The ARG dye wastewater is characterized mainly by high colority and resistance to biodegradation [30]. Hence, the removal of ARG dye from aqueous solutions is required.

Therefore, the removal efficiency (RE) of the novel porous ceramsite for ARG dye from aqueous solutions in batch and fixed-bed column experiments was discussed in this study. First, an orthogonal experimental design of five factors and four levels was conducted, and then the optimal condition of preparation was determined. Second, the adsorption equilibrium, adsorption kinetics, and thermodynamics of ARG dye on as-prepared porous ceramsite in batch experiments were investigated. Finally, the removal of ARG dye from aqueous solutions by a fixed-bed column packed with porous ceramsite was performed.

2 Materials and methods

2.1 Materials and reagents

Municipal sludge, coal fly ash, and river sediment were supplied by Shanghai Songjiang Sewage Treatment Plant, Shanghai Waigaoqiao Power Generation Co., Ltd, and Songjiang Campus of Donghua University, China,

respectively. Chemical reagents, such as sodium metasilicate (Na_2SiO_3), calcium carbonate ($CaCO_3$), hydrochloric acid (HCl), sodium hydroxide (NaOH), sodium chloride (NaCl), and polyvinyl alcohol (PVA) (CH_2CHOH)_n, were provided by Sinopharm Chemical Reagent Co., Ltd, China. Experiments were conducted with the aid of distilled water. All the experiments were carried out under atmospheric pressure.

ARG dye of analytical grade was supplied by the Chinese company Sinopharm Chemical Reagent Co., Ltd. Its chemical structure is shown in Figure 1. All the ARG dye solutions used in this research were prepared by weighing and dissolving the required amounts of ARG dye in distilled water. Besides, the linear relationship between the absorbance at 505 nm and the ARG dye concentration is shown in Figure 1, which indicated that there is a good linear relationship between them, with $R^2 = 0.9998$.

2.2 Preparation

In our previous research, the high contents of SiO_2 , Al_2O_3 , Fe_2O_3 , and CaO came from municipal sludge (7.5%, 2.3%, 6.9%, and 2.9%, respectively), coal fly ash (56.8%, 25.7%, 7.0%, and 8.1%, respectively), and river sediment (52.5%, 17.6%, 5.1%, and 1.5%, respectively), which met the material requirements for the preparation of porous ceramsite by sintering method [31,32], and their optimal mass ratio was 5:1:4 [24]. However, there are many complicated influence factors during the preparation process, which may affect the properties of porous ceramsite. Therefore, an orthogonal experimental design of five factors, including PVA additive, preheating and sintering temperature, as well as preheating and sintering time,

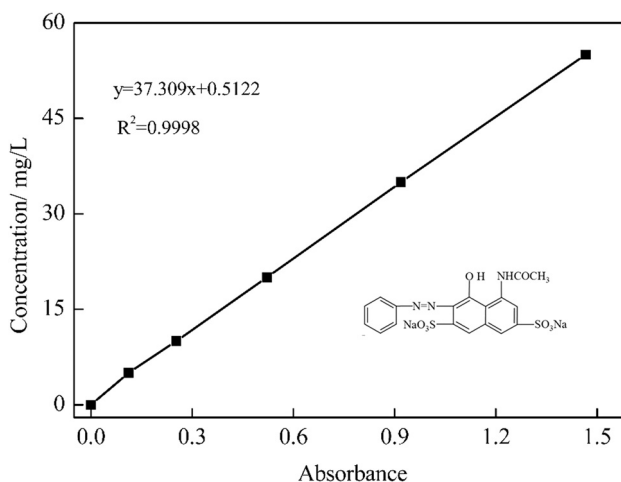


Figure 1: The standard curve of ARG dye concentration (x) versus absorbance (y) and its chemical structure.

and four levels were conducted to optimize the process parameters (Table 1). Meanwhile, the void fraction of porous ceramsite was used as the evaluation index.

The Na_2SiO_3 and CaCO_3 were added to the mixture after weighted and both of their final doses were 5% (per 100 g mixture), and they were placed in a glass beaker containing 40 mL of PVA solution (per 100 g mixture) and distilled water to obtain adequate plasticity. Subsequently, the green bodies with a diameter of 10 mm were prepared and dried at room temperature, as shown in Figure 2a1. Then, sintering treatment was carried on a pipe furnace (provided by SX2-6-13, Shanghai Yifeng Electric Furnace Co., Ltd, China). Finally, the porous ceramsite was gained after natural cooling, as shown in Figure 2a2.

Furthermore, after crushing and sieving, the porous ceramsite with a diameter of 0.5 ± 0.2 mm was obtained for the better absorption of target pollutants in subsequent experiments [33]. Meanwhile, to enhance the adsorption capacity of the porous ceramsite [34], they were placed into 1 mol/L NaCl solution (1 g:10 mL), stirred 120 min (120 rpm) with a magnetic stirrer at 80°C, and dried at 80°C for about 8 h after washing with deionized water for several times.

2.3 Batch experiment

Efforts had been exerted in batch tests on selected reaction temperature ranging from 278–318 K. Two grams of porous ceramsite were added to 100 mL of ARG dye solution, and the initial concentration was set as 5 mg/L and initial pH as 3 in a glass beaker. Then the beaker was stirred (150 rpm) with a magnetic stirrer at a given time interval. Measurement for ARG dye concentration in the filtrate was completed in condition of the maximum wavelength of 505 nm. The ARG dye uptake at equilibrium (q_e) and the quantity adsorbed at time t (q_t) are calculated respectively as follows [35]:

$$q_t = \frac{(C_0 - C_t)V}{m}, \quad (1)$$

$$q_e = \frac{(C_0 - C_e)V}{m}, \quad (2)$$

where C_0 , C_e , and C_t are the concentration of the ARG dye solution at initial, equilibrium, and time t , respectively, mg/L; V is the volume of the solution, L; and m is the weight of the porous ceramsite, g.

Table 1: Results of $L_{16} (4)^5$ orthogonal experiments for the preparation of porous ceramsite

No.	PVA (%)	Preheating temperature (°C)	Preheating time (min)	Calcining temperature (°C)	Calcining time (min)	Void fraction (%)
1	0.1	200	10	1,050	2	56.7
2	0.1	300	20	1,100	5	60.1
3	0.1	400	30	1,150	7	69.4
4	0.1	500	40	1,200	10	77.7
5	0.5	200	20	1,150	10	66.4
6	0.5	300	10	1,200	7	75.5
7	0.5	400	40	1,050	5	59.4
8	0.5	500	30	1,100	2	61.8
9	0.9	200	30	1,200	5	75.1
10	0.9	300	40	1,150	2	66.8
11	0.9	400	10	1,100	10	64.6
12	0.9	500	20	1,050	7	61.3
13	1.3	200	40	1,100	7	60.0
14	1.3	300	30	1,050	10	62.2
15	1.3	400	20	1,200	2	77
16	1.3	500	10	1,150	5	70.1
K1	65.98	64.55	66.73	59.9	65.58	
K2	65.78	66.15	65.45	61.63	66.18	
K3	66.95	67.6	67.13	68.18	66.55	
K4	67.32	67.73	65.98	76.32	67.73	
r	1.54	3.18	1.68	16.42	2.15	

K is the value for each level of a parameter and is the average of four void fraction values; r is the range value for each factor and is the difference between the maximal and minimal K values.

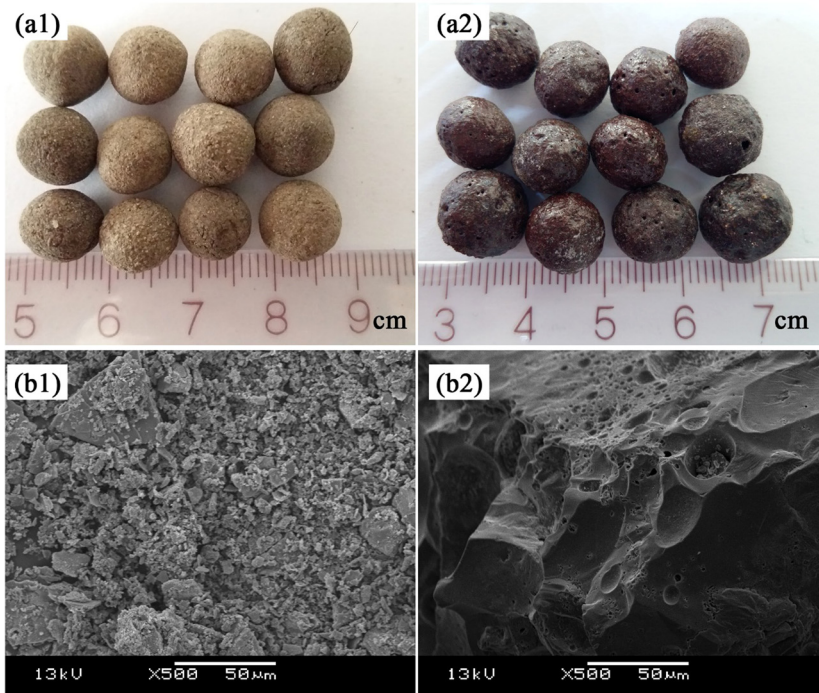


Figure 2: Pictures (a1: green bodies, a2: porous ceramsites) and SEM images (b1: green bodies, b2: porous ceramsites) of samples.

2.4 Column experiment

Experimental site was chosen to be a neat cylindrical glass tube for conducting tests on fixed-bed column (internal diameter, 14.0 cm; column height, 100.0 cm; volume, $4.4 \times 10^3 \text{ cm}^3$), in which a piece of filter cloth was placed respectively at the top and bottom of the tube to avoid the penetration of packing, and a certain amount of porous ceramsite was packed into the tube (schematic diagram is shown in Figure 3). The ARG dye wastewater with initial pH value of 3, initial concentration of 5 mg/L, and inlet flow rate of 33 mL/min entered the column via the base, and the column had an in-built variant peristaltic pump. The top of the column was designed to discharge efflux through a discharge pipe connected to a collection tank. The starting time was set to be the node at which the efflux was discharged. The reaction temperatures were set at $5 \pm 2^\circ\text{C}$, $25 \pm 2^\circ\text{C}$, and $45 \pm 2^\circ\text{C}$, respectively.

2.5 Analysis

Measurement for the void fraction of porous ceramsite adhered to the Standard Methods of Artificial Ceramsite Filter Material for Water Treatment in China (CJ/T 299-

2008). The measurement of scanning electron microscopy (SEM) and X-ray diffraction (XRD) had been detailed in our previous report [36].

Breakthrough curves (BTCs) indicate ARG dye's loading effect onto the column and are expressed by the proportion between effluent ARG dye concentration and influent ARG dye concentration (C_t/C_0). In particular, the ratio is actually computed as the time function. In a condition that C_t approaches 5% approximately, with C_0 being the breakthrough point (as $C_t = 5\% C_0$), then its time equates to the time of breakthrough. Correspondingly, in a condition that C_t approaches 90%, with C_0 being the exhaustion point as $C_t = 90\% C_0$, then its time equates to the time of saturation. The ARG dye RE in fixed-bed column packed with porous ceramsite can be calculated with Eq. 3. The cumulative retention curves (CRCs) show the total mass of ARG dye adsorbed onto porous ceramsite (mg/g) as a function of empty bed volumes of flow passing through the column and can be calculated with Eq. 4 [37].

$$\text{RE} = \frac{C_0 - C_t}{C_0} \times 100\%, \quad (3)$$

$$q_i = \frac{v \sum_{i=1}^n (C_0 - C_i) \Delta t_i}{m}, \quad (4)$$

where C_0 , C_t , and C_i are initial concentration, concentration at t time, and average effluent concentration between time t_i and t_{i-1} , mg/L; v is the flow rate, L/min; m is the

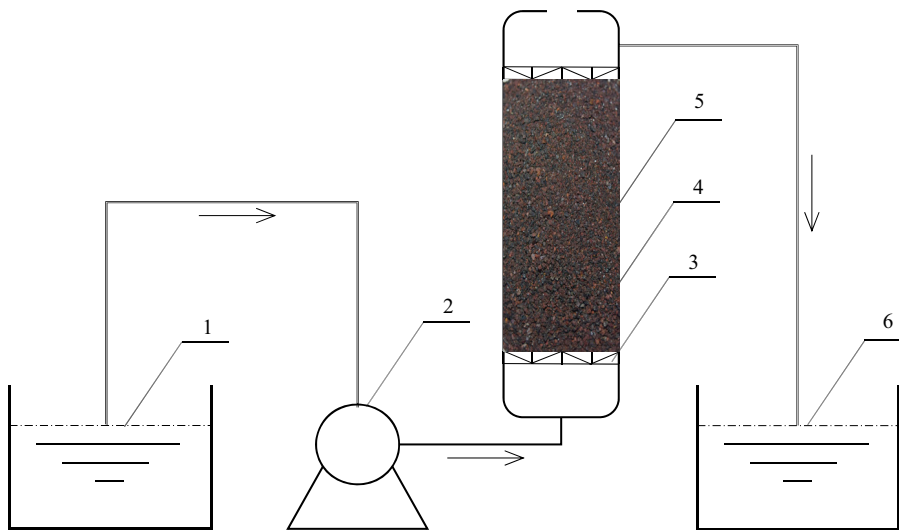


Figure 3: Schematic diagram of the fixed-bed column system (1 – influent tank, 2 – peristaltic pump, 3 – filter cloth, 4 – porous ceramsites, 5 – fixed-bed column, 6 – effluent tank).

weight of porous ceramsite, g ; and Δt_i is the time difference ($t_i - t_{i-1}$), min.

To evaluate if the empirical data conform to the data estimated by the model, the root mean-square error (RMSE) and chi-square examination (χ^2) are calculated with Eq. 5 and 6, respectively [38].

$$\text{RMSE} = \sqrt{\frac{1}{n-p} \sum_{i=1}^n (X_{\text{exp}} - X_{\text{cal}})_i^2}, \quad (5)$$

$$\chi^2 = \sum_{i=1}^n \left[\frac{(X_{\text{exp}} - X_{\text{cal}})_i^2}{X_{\text{cal}}} \right], \quad (6)$$

where X_{exp} and X_{cal} are the experimental data and calculated data, respectively; n is the number of experimental data points; and p is the number of the parameters within model equations.

3 Results and discussion

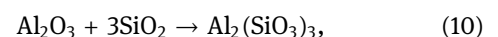
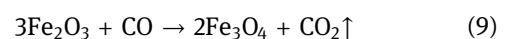
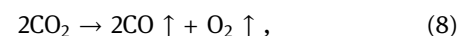
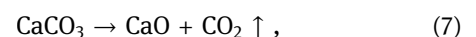
3.1 Preparation and characterization

3.1.1 Orthogonal experiment

Table 1 shows that the investigated factors with different levels had evident influence on the value of void fraction of porous ceramsite. In detail, the void fraction was very sensitive to sintering temperature, whereas it was

insensitive to PVA additive, as indicated by the value of r . The range analysis indicated that the sintering temperature was the most important factor, followed by preheating temperature, sintering time, preheating time, and PVA additive. Furthermore, Table 1 also indicates that the optimal PVA additive was 0.1 wt%, ideal temperature and time for preheating should be set as 400°C and 30 min, and those for sintering treatment should be 1,150°C and 7 min.

The sintering temperature was the primary determinant, mainly because pyrolysis reactions occurred under high-temperature conditions (700–1,000°C) and a proper amount of sintered gases were produced in the internal ceramsite billet, as shown in Eq. 7–9. Sintered gases are a requisite for sintering preparation of ceramsite. In addition, under high-temperature conditions (>1,000°C), crystal lattice was transformed, as shown in Eq. 10–12, and a suitable viscous liquid phase appeared in ceramsite billet surface. The suitable viscous liquid phase is also another necessary condition for the sintering preparation of ceramsite.



3.1.2 Characterization

Under the abovementioned optimal conditions of preparation (0.1 wt% PVA additive, preheating at 400°C for 30 min, and sintering at 1,150°C for 7 min), the porous ceramsite was prepared from solid wastes, then it was characterized by SEM and XRD, and the results are presented in Figures 2 and 4, respectively.

Figure 2 shows that the color and morphology of the samples were significantly different. Figure 2a1 shows that the colors of the samples were changed from grayish yellow to brick red after sintering. Meanwhile, the surface of the samples turned from rough to smooth and porous, as shown in Figure 2a2. Furthermore, SEM images obviously outlined that green bodies were on uneven surface and in discrete framework, as shown in Figure 2b1. By contrast, Figure 2b2 shows that the surface of the samples would be progressively tightened after high-temperature sintering, and where irregular forms were combined, with hollow patterns. The reasons are mainly because of the fact that melting and blending took place between the components of raw materials at high sintering temperature, resulting in densification [39].

As Figure 4 shows that there is large disparity in XRD spectra between green body and porous ceramsite, which reflect sintering temperature is extremely important in the preparation process. Comparing the XRD spectra of different samples suggested that the peak intensity of the samples was significantly reduced, but the peak height was flat and the peak noise was obvious, as shown in Figure 4b. In addition, as seen in Figure 4a, the mineralogical compositions in green body were relatively single and mainly consisted of quartz and iron oxides, whereas albite, anorthite, and labradorite could be detected in porous ceramsite (Figure 4b).

3.2 Batch study

3.2.1 Adsorption equilibrium

Adsorption isotherms mean a lot in the treatment of wastewater. That is attributed to its capacity of studying how the equilibrium adsorption capacity is correlated with the equilibrium concentration at a certain reaction temperature. Besides, many equations, such as the ones proposed by Langmuir and Freundlich, had gained application in determining adsorption equilibrium. Thus, the values of q_m , K_L , K_F , $1/n$, R^2 , RMSE, and χ^2 were examined at 278, 298, and 318 K (Table 2). It was found that at different reaction

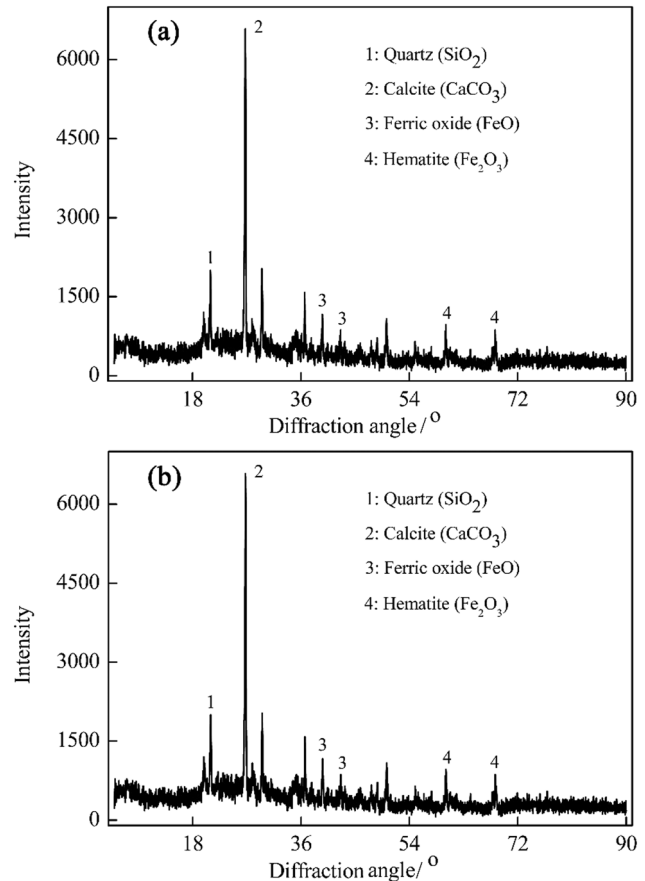


Figure 4: XRD spectra of green body (a) and porous ceramsite (b).

temperatures, the adsorption equilibrium of ARG dye on porous ceramsite is up to the Freundlich isotherm model, with high R^2 values (>0.997) and low values of RMSE and χ^2 , indicating that the adsorption process is reversible, thus resulting in higher adsorptive capacity, and the energy distribution is not uniform and multiple layers are commonly formed [40]. Table 2 also displays that Langmuir isotherm model can adequately describe the equilibrium of ARG dye adsorption on porous ceramsite ($R^2 > 0.96$ and $\chi^2 < 0.019$).

In case that reaction temperature increases to 318 K from 298 K, the value of q_m calculated with the Langmuir model increased from 9.625 to 10.695 mg/g, whereas the value of R^2 decreased from 0.992 to 0.977, thus weakening the linear relationship. The K_L values obtained from this experiment at all the tested reaction temperatures were in the range of 1.19×10^{-2} to 1.47×10^{-2} L/mg, showing that the adsorption of ARG dye on porous ceramsite was favorable at all the tested reaction temperatures [41]. In addition, the value of $1/n$ in the study was more than 1, suggesting the adsorption process on porous ceramsite's uneven surface and was a monolayer homogeneous adsorption process.

Table 2: Adsorption isotherm, kinetic, and thermodynamic parameters for ARG dye removal by porous ceramsite at different reaction temperatures

Properties	Model	Parameter	Reaction temperature			
			278 K	298 K	318 K	
Isotherms	Langmuir $\frac{C_e}{q_e} = \frac{1}{q_m K_L} + \frac{C_e}{q_m}$	q_m	8.511	9.625	10.695	
		$K_L \times 10^{-2}$	1.19	1.47	1.37	
		R^2	0.962	0.992	0.977	
		RMSE	1.03	0.897	0.796	
		χ^2	1.9×10^{-2}	1.9×10^{-2}	1.6×10^{-2}	
	Freundlich $\ln q_e = \ln K_F + \frac{1}{n} \ln C_e$	K_F	2.42	2.43	2.41	
		$1/n$	2.2	1.9	1.8	
		R^2	0.999	0.998	0.997	
		RMSE	0.68	0.683	0.636	
		χ^2	0.914	0.45	0.276	
Kinetics	Pseudo-first-order $\ln(q_e - q_t) = \ln q_e - \frac{K_1 t}{2.303}$	$K_1 \times 10^{-3}$	8.06	5.76	6.91	
		q_e	4.104	4.955	4.436	
		R^2	0.959	0.994	0.993	
		RMSE	0.147	0.128	0.153	
		χ^2	1.7×10^{-3}	1.5×10^{-3}	2.2×10^{-3}	
	Pseudo-second-order $\frac{t}{q_t} = \frac{1}{K_2 q_e^2} + \frac{t}{q_e}$	K_2	0.131	0.234	0.184	
		q_e	0.177	0.277	0.349	
		R^2	0.932	0.927	0.918	
		Intraparticle diffusion $q_t = K_p t^{\frac{1}{2}} + C$	$K_p \times 10^{-3}$	6.2	7.5	9.6
		R^2	0.984	0.998	0.999	
Thermodynamics	$K_D = \frac{V(C_0 - C_e)}{m C_e}$ $\Delta G^0 = -RT \ln K_D$ $\Delta G^0 = \Delta H^0 - T \times \Delta S^0$	K_D	3.589	3.439	3.248	
		ΔG^0	-2.954	-3.06	-3.115	
		ΔH^0		-1.844		
		ΔS^0		4.0×10^{-3}		
		χ^2	9.0×10^{-4}	7.0×10^{-4}	6.0×10^{-4}	

C_0 is the initial concentration of ARG dye in the influent, mg/L; C_e is the concentration of ARG dye at equilibrium, mg/L; q_e is the amount of adsorbed ARG dye per unit porous ceramsite mass, mg/g; q_t is the amount of ARG dye adsorbed at time t , mg/g; q_m is the maximum monolayer adsorption capacity, mg/g; K_L is the Langmuir equilibrium constant, L/mg; K_F is the Freundlich equilibrium constant, mg/g; $1/n$ is the heterogeneity factor; K_1 is the rate constant of the pseudo-first-order reaction kinetic, g/min mg; K_2 is the rate constant of the pseudo-second-order reaction kinetic, g/min mg; K_p is the rate constant of the intraparticle diffusion model, mg/g min^{1/2}; C is the intercept; R^2 is the correlation coefficient; K_D is the solid-liquid partition coefficient, mL/g; ΔG^0 is the Gibbs free energy, kJ/mol; ΔH^0 is the enthalpy, kJ/mol; ΔS^0 is the entropy, kJ/mol; R is the gas constant, 8.314 J/mol K; T is the Kelvin temperature, K; V is the volume of ARG dye solution, L; m is the weight of porous ceramsite, g.

3.2.2 Adsorption kinetics

Adsorption kinetics modeling can provide insights into both the rate of adsorption and the control of rate of the adsorption process [42]. To evaluate the adsorption process of ARG dye from aqueous solutions using porous ceramsite, several well-known adsorption models, such as Lagergren pseudo-first-order model, Ho's pseudo-second-order model, and intraparticle diffusion kinetic model, were used for exploring the batch experimental data.

Table 2 shows that the q_e values calculated according to the pseudo-first-order model was more in proximity to

the experimental value of q_e than that computed by the pseudo-second-order model at all reaction temperatures. R^2 of the pseudo-first-order model was close to 0.96, which was larger than that of pseudo-second-order model. Moreover, Table 2 indicates that the value of the pseudo-first-order reaction kinetic rate constant (K_1) was almost ten times higher than the value of the pseudo-second-order reaction kinetic rate constant (K_2) within the investigated reaction temperature range, manifesting the role of the physical adsorption as part of the adsorption process, and that some other mechanisms might also play an important role in the adsorption process. Therefore, the pseudo-first-order

kinetics could be approximated well as a favorable model for ARG dye adsorption onto porous ceramsite.

In the intraparticle diffusion model, the straight line of the intraparticle region did not pass through the origin, certifying that ARG dye adsorption on porous ceramsite involved two steps. ARG dye molecules in the solution were shifted to the exterior of porous ceramsite during the first procedure, known as film diffusion, thus attributing to diffusion at the boundary layer. In the second step (known as intraparticle diffusion), ARG dye molecules were passed through the abundant voids of cross-linked porous ceramsite because of the intraparticle diffusion effects and gradual equilibrium stage. It should be pointed out that the film diffusion and the intraparticle diffusion might occur simultaneously [43,44].

3.2.3 Adsorption thermodynamics

Thermodynamic parameters, such as ΔG^0 , ΔH^0 , and ΔS^0 , for the adsorption of ARG dye with porous ceramsite were measured at 278, 298, and 318 K. As seen in Table 2, the ΔG^0 values were less than 0.0 kJ/mol at all reaction temperatures, indicating the spontaneity of ARG dye's adsorption on porous ceramsite. Furthermore, the ΔG^0 varied between -20.0 and 0.0 kJ/mol, showing that the removal of ARG dye was a physical adsorption process. Besides, the value of ΔG^0 decreased monotonically with the increase in reaction temperature (Table 2), suggesting that the energy required for ARG dye to bind to porous ceramsite at low reaction temperature was less than that at high reaction temperature.

Negativity of ΔH^0 confirmed that the adsorption process of ARG dye with porous ceramsite was an exothermic reaction. In other words, much heat was released to accelerate the adsorption process of the whole system. Positive ΔS^0 values indicated that the adsorption process of ARG dye by porous ceramsite was an entropy increase process. The increased randomness and affinity in the adsorption of ARG dye on porous ceramsite at the solid/solution interface would be established.

3.3 Column study

The observation results of the adsorption process in the dynamic systems better reflected the dynamic behaviors,

involving breakthrough and saturation times, column space, and length, in environmental applications, because liquid flow and complex mass transport are considered [45].

3.3.1 Effect of initial pH

The effect of initial pH on ARG dye removal from aqueous solutions by a fixed-bed column packed with porous ceramsite was evaluated at various initial pH values (3–11) (Figure 5). With the increase in initial pH, breakthrough and saturation times were right-skewed to flatten the profile of BTC, as shown in Figure 5a. In a condition that the initial pH changed from 3 to 11, the time of breakthrough was simultaneously prolonged from 510 to 720 min. Saturation time showed a similar tendency in the whole investigated range. In short, a decrease in the BTC slope was also observed, indicating an enlargement of the mass transfer region. The breakthrough and saturation points occurred more lately under acidic conditions than under alkaline conditions.

Figure 5b shows that the RE of ARG dye was highly affected by the initial pH. The maximum RE occurred at the lowest initial pH, implying that the acidic condition promoted the removal of ARG dye from aqueous solutions by the fixed-bed column packed with porous ceramsite. It might be interpreted as follows: after pretreatment with NaCl solution, the hydrogen element in $-OH$ was replaced by Na^+ ion on the surface of porous ceramsite, following a cation exchange reaction occurred between ARG dye molecule and Na^+ ion [32]. When the operating time was shorter than 510 min, the value of RE always exceeded 90.2%. However, it became much slower when the operating time increased from 510 to 990 min. After operating for 990 min, the value of RE was a constant, indicating that the adsorption equilibrium was reached.

Moreover, ARG dye removal from aqueous solutions by the fixed-bed column packed with porous ceramsite was characterized by a symmetrical S-shaped CRC within the investigated initial pH range. Figure 5c shows that the value of CRC was 34.74 mg ARG dye per gram under acidic conditions (initial pH was 3), which was 8.32% higher than that under neutral conditions (initial pH was 7) and 28.7% higher than that under alkaline conditions (initial pH was 11). The cumulative ARG dye captured by the fixed-bed column after exhaustion was roughly 3.61 times higher than the maximal adsorption capacity of the Langmuir obtained from the batch experiment.

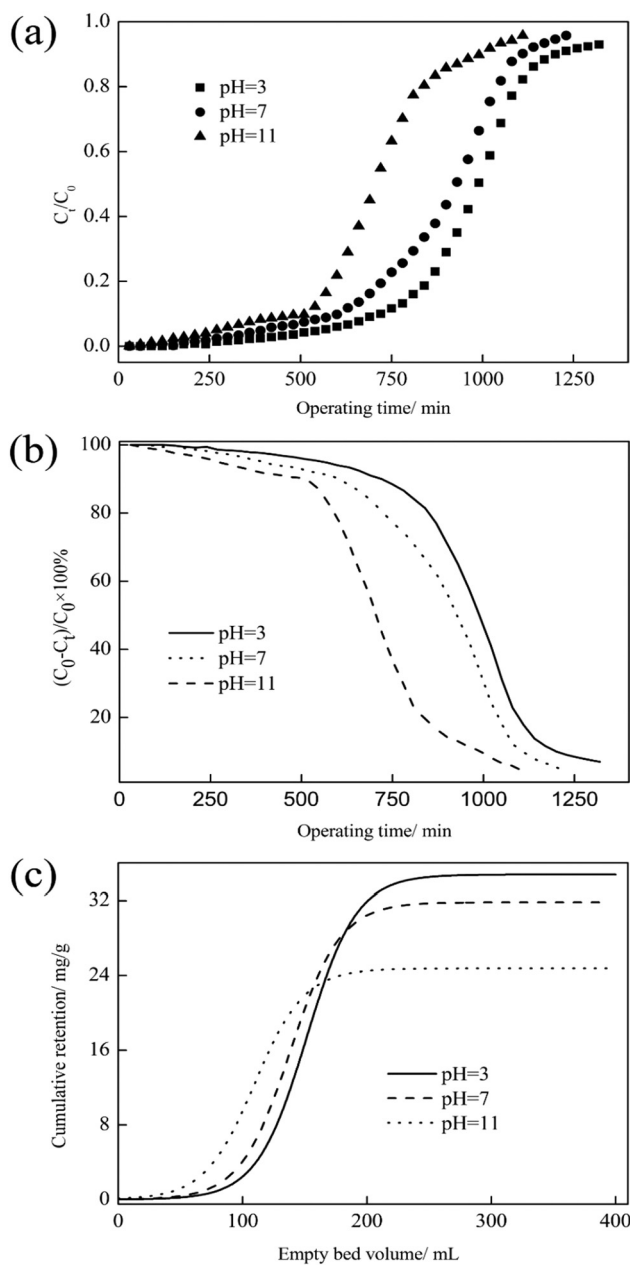


Figure 5: Effect of initial pH on the removal of ARG dye from aqueous solutions by fixed-bed column packed with porous ceramsite. Experimental conditions: reaction temperature was set at 25°C and initial concentration at 5 mg/L. (a) BTCs, (b) RE, and (c) CRCs.

3.3.2 Effect of reaction temperature

The reaction temperature is considered an important design parameter of fixed-bed column mainly because of temperature-induced changes in the mass transfer of packings [46]. Therefore, the effect of reaction temperature on ARG dye removal from aqueous solutions by the fixed-bed column packed with porous ceramsite was

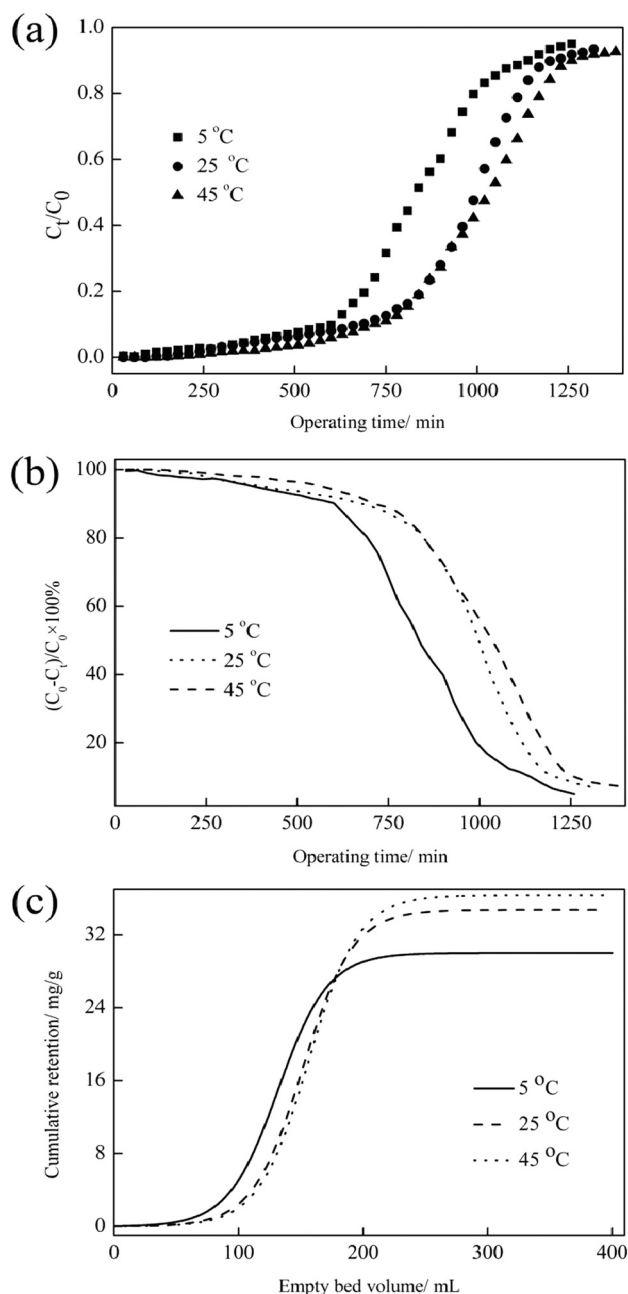


Figure 6: Effect of reaction temperature on the removal of ARG dye from aqueous solutions by fixed-bed column packed with porous ceramsite. Initial pH was set at 3.0 and initial concentration at 5 mg/L. (a) BTCs, (b) RE, and (c) CRCs.

evaluated by BTCs, RE, and CRCs in this study. Figure 6a shows that the BTC became gentler with the increase in treatment time. In a condition that the reaction temperature increases from 5°C to 45°C, the corresponding time of breakthrough was prolonged from 600 to 720 min. A similar trend was also found in saturation time. This is principally because of the increased mass transfer

thickness layer around the porous ceramsite induced by rising of reaction temperature [47].

Figure 6b shows that the value of RE exhibited a downward trend in the investigated reaction temperature range. When the operating time increased from 0 to 600 min, the value of RE decreased by only about 8%. However, when the operating time increased from 600 to 1,140 min, the value of RE decreased rapidly. On the contrary, after operating for more than 1,140 min, the value of RE became stable, suggesting that the saturation point was reached. This may be attributed to the fact that with the increase in the operating time, the saturation point of packing was reached earlier, thus decreasing the treatment efficiency of fixed-bed column.

Figure 6c shows the concurrent rise in CRCs of ARG dye with growing high reaction temperature. Although the increase in reaction temperature consolidated mass transfer rate, the CRCs of ARG dye on porous ceramsite increased slowly because all the surface of porous ceramsite were not accessible to the dye molecules.

3.3.3 Kinetic analysis

A prediction model that describes and analyzes the lab-scale fixed-bed column counts much to industrial application [48]. Therefore, to better investigate the removal performance of ARG dye from aqueous solutions by

porous ceramsite in a fixed-bed column, the Thomas, Yoon–Nelson (Y–N), and Adams–Bohart (A–B) models were used to fit the experimental data in Figures 5a and 6a, and the results are listed in Table 3.

Table 3 shows that both initial pH and reaction temperature affected the values of K_{TH} and K_{YN} , but the effect of initial pH was a prime dominant. As the initial pH value increased, K_{TH} increased and q_{total} decreased. The reason for this trend may be that with the increase in pH, acidic matters attached onto the adsorbent surface progressively neutralized and negative charges of adsorbents kept growing on the surface [49]. The q_{total} decreased as a function of initial pH value and increased as a function of reaction temperature, which increased from 45.95 to 55.48 mg/g with the reaction temperature increasing from 5°C to 45°C. Besides, a slight difference was observed between the predicted and experimental data of q_{total} , implying that the Thomas model could predict the breakthrough performance when initial pH or reaction temperature changed, without requiring additional experiments.

Table 3 indicates that the values of RMSE and χ^2 increased with the increase in initial pH, showing the consistency between model predictions and test results. With the increase in the reaction temperature, χ^2 was first decreased and then increased. As shown by the research results, the increase in τ led to the increase in reaction temperature, whereas it decreased with the increase in

Table 3: Parameters estimated by the Thomas, Y–N, and A–B models in various experimental conditions

Model	Parameter	Initial pH			Reaction temperature		
		3	7	11	5°C	25°C	45°C
Thomas $\ln\left(\frac{C_0}{C_0-C_t}\right) = K_{TH}C_0t - \frac{K_{TH}q_{total}m}{v}$	$K_{TH} \times 10^{-3}$	1.24	1.44	1.5	1.34	1.24	1.32
	q_{total}	52.98	47.34	38.68	45.95	52.91	55.48
	RMSE	2.055	2.572	2.592	2.675	2.051	2.581
	χ^2	0.046	0.105	0.177	0.121	0.046	0.09
	R^2	0.954	0.968	0.979	0.979	0.956	0.985
Y–N $\ln\left(\frac{C_0}{C_0-C_t}\right) = K_{YN}t - \tau K_{YN}$	$K_{YN} \times 10^{-3}$	6.2	7.2	7.5	6.7	6.2	6.6
	τ	953	861	703	835	958	1,009
	RMSE	2.383	2.51	2.594	2.604	2.384	2.521
	χ^2	0.046	0.105	0.177	0.114	0.046	0.083
A–B $\ln\left(\frac{C_t}{C_0}\right) = K_{AB}C_0t - K_{AB}N_0\left(\frac{Z}{U_0}\right)$	$K_{AB} \times 10^{-3}$	0.86	0.98	0.92	0.88	0.84	0.94
	N_0	2,001	1,797	1,585	1,821	2,001	2,018
	R^2	0.959	0.937	0.944	0.942	0.956	0.967
	RMSE	1.1888	1.749	1.848	1.798	1.188	1.763
	χ^2	0.018	0.03	0.035	0.033	0.018	0.032

C_0 is the initial concentration of ARG dye in the influent, mg/L; C_t is the concentration of ARG dye in the effluent at t min, mg/L; q_{total} is the maximum adsorption capacity, mg/g; K_{TH} is the Thomas rate constant, mL/min/mg; v is the volumetric flow rate, mL/min; K_{YN} is the Yoon–Nelson rate constant, min^{-1} ; τ is the time required for 50% packing breakthrough, min; K_{AB} is the Adams–Bohart kinetic constant, L/mg min; N_0 is the saturation concentration, mg/L; Z is the bed depth of fixed-bed column, cm; U_0 is the ratio of the volumetric flow rate to the cross-section from the beginning to the end of breakthrough.

initial pH, suggesting that increasing reaction temperature and reducing initial pH slowed down adsorption saturation and prolonged breakthrough time. Interestingly, the value of N_0 was proportional to the initial pH value, but inversely proportional to reaction temperature, determining that the removal performance of the fixed-bed column packed with porous ceramsite depended heavily on internal mass transfer.

Taking together, the high value of R^2 and low values of RMSE and χ^2 indicated that the Y–N model showed better adsorption behavior of the fixed-bed column packed with porous ceramsite compared with Thomas model or A–B model, providing a valuable design tool for column adsorption.

4 Conclusions

In this study, a novel porous ceramsite was prepared from solid wastes by sintering process, and then its batch and fixed-bed column performances for ARG dye removal from aqueous solutions were studied. Under the optimal condition of preparation (0.1 wt% PVA additive, pre-heating at 400°C for 30 min, and sintering at 1,150°C for 7 min), the porous ceramsite can be prepared from municipal sludge, coal fly ash, and river sediment, with exhibits developing pore structure and high specific surface area.

The adsorption kinetics of batch tests adhered to the pseudo-first-order model, with its equilibrium compliant with the Freundlich–Langmuir isotherm. In the dynamic adsorption process for fixed-bed column packed with porous ceramsite, breakthrough and exhaustion times were both decreased as the initial pH went up, and the curves grew concurrently with the rising reaction temperature. Compared with batch experiment, the treatment effect and capacity could be greatly improved in the fixed-bed column stage, which is even more close to the industry practice. This study showed that the as-prepared porous ceramsite could be used as an efficient and alternative water treatment material for the removal of ARG dye from aqueous solutions.

Acknowledgments: This research was supported by the Natural Science Foundation Training Project of Shandong Province, China (Grant No. ZR2018PEE026), Shandong Key Laboratory of Water Pollution Control and Resource Reuse (Grant No. 2019KF05), and Postdoctoral Science Foundation of Henan Province (Grant No. 1902036).

References

- [1] Chen M, Li ZH, Wu JF, Wang JH. Shear behaviour and diagonal crack checking of shale ceramsite lightweight aggregate concrete beams with high-strength steel bars. *Constr Build Mater.* 2020;249:118730–9.
- [2] Li X, Shi XS, Yang ZM, Xu XH, Guo RB. Effects of recyclable ceramsite as the porous bulking agent during the continuous thermophilic composting of dairy manure. *J Clean Prod.* 2019;217:344–51.
- [3] Che TK, Pan BF, Ouyang J. The laboratory evaluation of incorporating ceramsite into HMA as fine aggregates. *Constr Build Mater.* 2018;186:1239–46.
- [4] Dong JX, Wang YH, Wang LJ, Wang SJ, Li SJ, Ding Y. The performance of porous ceramsites in a biological aerated filter for organic wastewater treatment and simulation analysis. *J Water Process Eng.* 2020;34:101134–43.
- [5] Fu PF, Lin XF, Chen ZH. Porous Fe^0/C ceramsites for removal of aqueous $\text{Pb}(\text{II})$ ions: Equilibrium, long-term performance and mechanism studies. *RSC Adv.* 2018;8:25445–55.
- [6] Li XG, Wang PQ, Qin JY, Liu YX, Qu YA, Liu JJ. Mechanical properties of sintered ceramsite from iron ore tailings affected by two-region structure. *Constr Build Mater.* 2020;240:117919–27.
- [7] Wu HQ, Zhang T, Pan RJ, Chun YY, Zhou HM, Zhu WX, et al. Sintering-free preparation of porous ceramsite using low-temperature decomposing pore former and its sound-absorbing performance. *Constr Build Mater.* 2018;171:367–76.
- [8] Jiang C, Jia LY, Zhang B, He YL, Kirumba G. Comparison of quartz sand, anthracite, shale and biological ceramsite for adsorptive removal of phosphorus from aqueous solution. *J Env Sci.* 2014;26:466–77.
- [9] Zhuang YZ, Chen CY, Ji T. Effect of shale ceramsite type on the tensile creep of lightweight aggregate concrete. *Constr Build Mater.* 2013;46:13–18.
- [10] Zhao HL, Liu F, Liu HQ, Wang L, Zhang R, Hao Y. Comparative life cycle assessment of two ceramsite production technologies for reusing municipal solid waste incinerator fly ash in China. *Waste Manage.* 2020;113:447–55.
- [11] Chen S, Qin CX, Wang T, Chen FY, Li XL, Hou HB, et al. Study on the adsorption of dyestuffs with different properties by sludge-rice husk biochar: Adsorption capacity, isotherm, kinetic, thermodynamics and mechanism. *J Mol Liq.* 2019;285:62–74.
- [12] Fan YJ, Zhu W, Gong M, Su Y, Zhang HW, Zeng JN. Catalytic gasification of dewatered sewage sludge in supercritical water: Influences of formic acid on hydrogen production. *Int J Hydrog Energ.* 2016;41:4366–73.
- [13] Xu XZ, Cao D, Wang ZH, Liu J, Gao J. Study on ultrasonic treatment for municipal sludge. *Ultrason Sonochem.* 2019;57:29–37.
- [14] Bianchini A, Bonfiglioli L, Pellegrini M, Sacconi C. Sewage sludge drying process integration with a waste-to-energy power plant. *Waste Manage.* 2015;42:159–65.
- [15] Wang XK, Zheng GD, Chen TB, Nie EQ, Wang YW, Shi XX, et al. Application of ceramsite and activated alumina balls as recyclable bulking agents for sludge composting. *Chemosphere.* 2019;218:42–51.
- [16] Tan P, Ma L, Fang QY, Zhang C, Chen G. Application of different combustion models for simulating the cocombustion of sludge

- with coal in a 100 MW tangentially coal-fired utility boiler. *Energy Fuel*. 2016;30:1685–92.
- [17] Jiang Y, Deng T, Yang K, Wang HY. Removal performance of phosphate from aqueous solution using a high-capacity sewage sludge-based adsorbent. *J Taiwan Inst Chem E*. 2017;76:59–64.
- [18] Capodaglio AG, Callegari A. Feedstock and process influence on biodiesel produced from waste sewage sludge. *J Env Manage*. 2018;216:176–82.
- [19] Zhu SY, Fang S, Huo MX, Yu Y, Chen Y, Yang X, et al. A novel conversion of the groundwater treatment sludge to magnetic particles for the adsorption of methylene blue. *J Hazard Mater*. 2015;292:173–9.
- [20] Gong M, Zhu W, Xu ZR, Zhang HW, Yang HP. Influence of sludge properties on the direct gasification of dewatered sewage sludge in supercritical water. *Renew Energ*. 2014;66:605–11.
- [21] Cheng G, Li QH, Su Z, Sheng S, Fu J. Preparation, optimization, and application of sustainable ceramsite substrate from coal fly ash/waterworks sludge/oyster shell for phosphorus immobilization in constructed wetlands. *J Clean Prod*. 2018;175:572–81.
- [22] Li J, Yu GW, Xie SY, Pan LJ, Li CX, You FT, et al. Immobilization of heavy metals in ceramsite produced from sewage sludge biochar. *Sci Total Env*. 2018;628:131–40.
- [23] Cao WP, Wang YM, Sun L, Jiang JL, Zhang YQ. Removal of nitrogenous compounds from polluted river water by floating constructed wetlands using rice straw and ceramsite as substrates under low temperature conditions. *Ecol Eng*. 2016;88:77–81.
- [24] Li TP, Sun TT, Aftab TB, Li DX. Photocatalytic degradation of methylene blue in aqueous solution using ceramsite coated with micro-Cu₂O under visible-light irradiation. *Korean. J Chem Eng*. 2017;34:1199–207.
- [25] Wang M, Zhang GL, Pang T, Cai DQ, Wu ZY. Removal of anthracenemethanol from soil through a magnetic system assisted by ceramsite coated with nanoflower-structured carbon and preparation for its engineering application. *Chem Eng J*. 2017;328:748–58.
- [26] Liu Y, Zhao YF, Cheng W, Zhang T. Targeted reclaiming cationic dyes from dyeing wastewater with a dithiocarbamate-functionalized material through selective adsorption and efficient desorption. *J Colloid Interf Sci*. 2020;579:766–77.
- [27] Chethana M, Sorokhaibam LG, Bhandari VM, Raja S, Ranade VV. Green approach to dye wastewater treatment using biocoagulants. *ACS Sustain Chem Eng*. 2016;4:2495–507.
- [28] Samsami S, Mohamadi M, Sarrafzadeh MH, Rene ER, Firoozbahr M. Recent advances in the treatment of dye-containing wastewater from textile industries: Overview and perspectives. *Process Saf Env*. 2020;143:138–63.
- [29] Li HY, Liu SY, Zhao JH, Feng N. Removal of reactive dyes from wastewater assisted with kaolin clay by magnesium hydroxide coagulation process. *Colloid Surf A: Physicochem Eng Asp*. 2016;494:222–7.
- [30] Feng JT, Sun NN, Wu DY, Yang HH, Xu H. Preparation of Fe₃O₄-TiO₂-polypyrrole ternary magnetic composite and using as adsorbent for the removal of acid red G. *J Polym Env*. 2017;25:781–91.
- [31] Cheng G, Li QH, Su Z, Sheng S, Fu J. Preparation, optimization, and application of sustainable ceramsite substrate from coal fly ash/waterworks sludge/oyster shell for phosphorus immobilization in constructed wetlands. *J Clean Prod*. 2018;175:572–81.
- [32] Wang JL, Zhao YL, Zhang PP, Yang LQ, Xu HA, Xi GP. Adsorption characteristics of a novel ceramsite for heavy metal removal from stormwater runoff. *Chin J Chem Eng*. 2018;26:96–103.
- [33] Zhao D, Gao YN, Nie S, Liu ZC, Wang FZ, Liu P, et al. Self-assembly of honeycomb-like calcium-aluminum-silicate-hydrate (C-A-SH) on ceramsite sand and its application in photocatalysis. *Chem Eng J*. 2018;344:583–93.
- [34] Li TP, Sun TT, Aftab TB, Li DX. Adsorption isotherms, kinetics and thermodynamics of ammonium nitrogen from aqueous solutions using modified ceramsite and its regeneration performance. *Desalin Water Treat*. 2017;90:196–205.
- [35] Li TP, Sun TT, Li DX. Removal of methylene blue from aqueous solution by ceramsite filter media combined with high temperature calcination for regeneration. *Desalin Water Treat*. 2017;59:220–9.
- [36] Li TP, Sun TT, Li DX. Preparation, sintering behavior and expansion performance of ceramsite filter media from dewatered sewage sludge, coal fly ash and river sediment. *J Mater Cycles Waste*. 2018;20:71–9.
- [37] Sellner BM, Hua GH, Ahiablame LM. Fixed bed column evaluation of phosphate adsorption and recovery from aqueous solutions using recycled steel byproducts. *J Env Manage*. 2019;233:595–602.
- [38] Vali SA, Baghdadi M, Abdoli MA. Immobilization of polyaniline nanoparticles on the polyurethane foam derived from waste materials: A porous reactive fixed-bed medium for removal of mercury from contaminated waters. *J Env Chem Eng*. 2018;6:6612–22.
- [39] Chen T, Yan B. Fixation and partitioning of heavy metals in slag after incineration of sewage sludge. *Waste Manage*. 2012;32:957–64.
- [40] Silva PMO, Francisco JE, Cajé JCM, Cassella RJ, Pacheco WF. A batch and fixed bed column study for fluorescein removal using chitosan modified by epichlorohydrin. *J Env Sci Health*. 2018;53:55–64.
- [41] Razak NFA, Shamsuddin M, Lee SL. Adsorption kinetics and thermodynamics studies of gold(III) ions using thioctic acid functionalized silica coated magnetite nanoparticles. *Chem Eng Res Des*. 2018;130:18–28.
- [42] Zhao YX, Yang YN, Yang SJ, Wang QH, Feng CP, Zhang ZY. Adsorption of high ammonium nitrogen from wastewater using a novel ceramic adsorbent and the evaluation of the ammonium-adsorbed-ceramic as fertilizer. *J Colloid Interf Sci*. 2013;393:264–70.
- [43] Wong KT, Eu NC, Ibrahim S, Kim H, Yoon Y, Jang M. Recyclable magnetite-loaded palm shell-waste based activated carbon for the effective removal of methylene blue from aqueous solution. *J Clean Prod*. 2016;115:337–42.
- [44] Chen ZH, Fu JW, Wang MH, Wang XZ, Zhang JA, Xu Q. Adsorption of cationic dye (methylene blue) from aqueous solution using poly (cyclotriphosphazene-co-4,4-sulfonyl-diphenol) nanospheres. *Appl Surf Sci*. 2014;289:495–501.
- [45] Cunha GC, Romão LPC, Santos MC, Araújo BR, Navickiene S, Pádua VL. Adsorption of trihalomethanes by humin: Batch and

- fixed bed column studies. *Bioresour Technol.* 2010;101:3345–54.
- [46] Ye YY, Yang J, Jiang W, Kang JX, Hu Y, Ngo HH, et al. Fluoride removal from water using a magnesia-pullulan composite in a continuous fixed-bed column. *J Env Manage.* 2018;206:929–37.
- [47] Li TP, Sun TT, Li DX. Removal of NH_4^+ -N from aqueous solution by ceramsite coated with $\text{Mg}(\text{OH})_2$ combined with air stripping. *Environ Eng Manage J.* 2019;18:727–35.
- [48] Li TP, Sun TT, Aftab TB, Li DX. Comparative study between ceramsite media and quartz sand for the removal of methylene blue dye from aqueous solution in fixed-bed columns. *Desalin Water Treat.* 2019;139:53–63.
- [49] Liu LH, Lin Y, Liu YY, Zhu H, He Q. Removal of methylene blue from aqueous solutions by sewage sludge based granular activated carbon: Adsorption equilibrium, kinetics, and thermodynamics. *J Chem Eng Data.* 2013;58:2248–53.